Check for updates

RESEARCH ARTICLE

Macromolecular Materials and Engineering
www.mame-journal.de

Electrospinning Ethanol–Water Solutions of Poly(Acrylic Acid): Nonlinear Viscosity Variations and Dynamic Taylor Cone Behavior

*Shameek Vats, Lawrence W. Honaker, Margaret W. Frey, Francesco Basoli, and Jan P.F. Lagerwall**

Electrospinning of polymer solutions is a multifaceted process that depends on the careful balancing of many parameters to achieve a desired outcome, in many cases including mixtures of multiple solvents. A systematic study of how the solution viscosity η—a good probe of solvent–polymer interactions—and the electrospinnability change when poly(acrylic acid) (PAA) is dissolved in ethanol–water mixtures at varying mixing ratio is carried out. A pronounced maximum is found in η at a water-to-ethanol molar ratio of about 2:1, where the solvent mixture deviates maximally from ideal mixing behavior and partial deprotonation of carboxyl groups by water coincides synergistically with dissolution of the uncharged protonated PAA fraction by ethanol. The PAA concentration is tuned as a function of water–ethanol ratio to obtain a common value of η for all solvent mixtures that is suitable for electrospinning. For high PAA content, the Taylor cone grows in volume over time despite minimum solution flow rate, even experiencing surface gelation for ethanol-rich solutions. This is attributed to the hygroscopic nature of PAA, drawing excess water into the Taylor cone from the air during spinning.

1. Introduction

Benefiting from its versatility, small equipment footprint, and ease in combining multiple materials within one and the same fiber, electrospinning[1–5] has become a popular technique for producing nonwoven mats of responsive and functionalized polymer fibers with very high specific surface area.[6,7] The diversity of properties is greatly expanded by incorporating functional liquids that are not spinnable on their own to make multifunctional composite fibers,[8–18] using coaxial electrospinning[19–22] or in situ phase separation.[23–25] Exhibiting manifold properties and significant tunability, these fibers are attractive to apply across many areas, for example, in sensing,[12,15,26–29] sound damping,[30] dynamic patterning,[31] thermal insulation via phase-change materials,[32,33] self-healing coatings,[34] or drug release.[35–39] However, success in spinning multifunctional composite fibers requires careful optimization of the polymer solvent with respect to the functional additive: otherwise, phenomena such as phase separation and gelation can disrupt the electrospinning process.[6,40] A common strategy (also in single-phase spinning) is to use mixtures of solvents, but many papers report only a fix solvent composition, without including any systematic study of how the polymer solution properties change with solvent mixing ratio. Given that a change in solvent composition can strongly affect the polymer–solvent interactions, there is good reason to carry out such a systematic study.

In this context, poly(acrylic acid) (PAA, **Figure 1**) is interesting, as it is readily soluble in water as well as ethanol,[41,42] allowing a complete study of how mixing these two solvents affects the PAA solution and its electrospinnability. Moreover, PAA is available in high molar mass suitable for electrospinning (as confirmed by several groups reporting successful PAA nano-/microfiber production[43–45]) and it can be made insoluble after spinning via chemical crosslinking,[43,44] of value for making fiber mats that withstand liquid immersion. The system of PAA dissolved in a water–alcohol mixture is also highly illustrative of the complexities that can arise with polymers dissolved in mixed solvents.

S. Vats, L. W. Honaker, J. P. Lagerwall
Department of Physics & Materials Science
University of Luxembourg
Luxembourg City 1511, Grand Duchy of Luxembourg
E-mail: jan.lagerwall@uni.lu

L. W. Honaker
Laboratory of Physical Chemistry and Soft Matter
Wageningen University & Research
Wageningen 6703 DE, The Netherlands

M. W. Frey
College of Human Ecology
Cornell University
Ithaca, NY 14853, USA

F. Basoli
Department of Engineering
Università Campus Bio-Medico di Roma
Rome 00128, Italy

The ORCID identification number(s) for the author(s) of this article can be found under https://doi.org/10.1002/mame.202100640

© 2021 The Authors. Macromolecular Materials and Engineering published by Wiley-VCH GmbH. This is an open access article under the terms of the Creative Commons Attribution License, which permits use, distribution and reproduction in any medium, provided the original work is properly cited.

DOI: 10.1002/mame.202100640

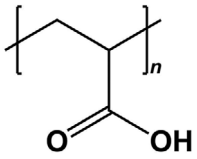

Figure 1. The structure of poly(acrylic acid) (PAA).

Studying water–ethanol solutions of polyvinylpyrrolidone (PVP), Guettari et al.[46] found that pure ethanol is a good solvent and water is a theta solvent (at the border between good and bad), while mixing reduced the performance in both directions, leading to a maximally poor solvent at about 70 mol% water. The same phenomenon was seen with water–methanol solutions of polyethylene oxide (PEO) by Shankar et al.,[47] who also demonstrated that the minimum of solvent quality coincides with a minimum of viscosity of the polymer solution. Both articles attributed the behavior to the solvent mixtures exhibiting a maximum deviation from ideal mixing behavior at a 2:1 molar ratio of water to alcohol due to competitive hydrogen bonding and formation of clusters with different solvent compositions at the molecular scale. In contrast to PVP and PEO, PAA is a polyion, that is, its pendant groups (carboxyl) are ionizable, and this can yield an even stronger sensitivity to the solvent properties. The high dielectric permittivity $\varepsilon_w \approx 78$ of water generally leaves polyions largely ionized,[48] giving rise to polyelectrolyte behavior.[49] Ethanol has a much lower permittivity than water, $\varepsilon_e \approx 25$, and we can thus expect significant counterion condensation and largely neutral PAA if it is dissolved in ethanol.

An interesting interplay between multiple phenomena should thus take place when electrospinning PAA dissolved in water–ethanol mixtures of varying compositions, because of the combined effects of a solvent changing character in a nonlinear way and the change from polyelectrolyte to neutral behavior of the solute. As a primary probe of solvent quality, we measure the shear viscosity η at low shear rate as a function of ethanol–water mixing ratio, confirming highly nonlinear behavior. To our surprise, however, PAA behaves opposite to PVP and PEO, with a maximum in η at intermediate solvent composition. This indicates that the mixed solvent has optimum properties for dissolving PAA, a finding that we attribute to the polyelectrolyte character of PAA when water is present in the solvent. We attempt to identify a PAA concentration c_{PAA} for each solvent composition that yields a value of η appropriate for electrospinning. The resulting variation in PAA concentration reveals the impact of yet another characteristic of PAA: its highly hygroscopic nature leads to significant water condensation from the air at high c_{PAA}, changing the ethanol–water balance in the Taylor cone, with strong impact on electrospinnability.

2. Results

2.1. Viscosity of PAA Solutions

The molar mass of our PAA is the same as that used by Li and Hsieh, who measured η as a function of c_{PAA} in pure water.[43] Replotting their data on a log–log scale (Figure S2, Supporting Information), a change of slope is easily recognized when c_{PAA} increases from 5% to 6% w/w. Fitting a power law function to the data, we find that the $\eta(c_{PAA})$ data are well reproduced with an exponent of 2 for c_{PAA} in the range 2–5% w/w, while, in the range 6–10% w/w, the exponent is 4.1. These exponents are well in line with the expectations for semidilute unentangled to semidilute entangled behavior, respectively[50]; hence we take c^e, $w_{PAA} \approx 5.5\%$ w/w as the critical entanglement concentration for PAA in water. This leads us to conduct our experiments with $c_{PAA} \geq 6\%$ w/w in order to have entangled solutions suitable for electrospinning.

We prepare solutions with $c_{PAA} = 6\%$, 7% , 8% , and 9% w/w in water–ethanol mixtures at 0% , 25% , 50% , 75%, and 100% w/w water, respectively, and measure η in a plate–plate rheometer as a function of oscillatory shear rate $\dot{\gamma}$. The full data are shown in the Supporting Information, Figures S3–S8, Supporting Information. Based on these data, we consider $\eta(\dot{\gamma} = 2.34\ s^{-1})$ a representative low-shear viscosity; lower $\dot{\gamma}$ gives poor measuring accuracy, possibly related to uncontrolled solvent evaporation during the long measuring time, with fluctuations in the apparent η. To get an overview of the behavior as function of water–ethanol molar ratio x_w ($x_w = 0$ corresponding to pure ethanol) as well as of c_{PAA}, we plot $\eta(\dot{\gamma} = 2.34\ s^{-1})$ as a function of x_w in **Figure 2** for $c_{PAA} = 6$, 7, and 9% w/w, respectively (see Supporting Information concerning the 8% w/w data). As an attempt to extrapolate between the experimental data points, we fitted a single-peak Gaussian function to each data set, yielding a good match to the obtained data.

The striking conclusion from Figure 2 is that all systems show a clear maximum in η for $x_w \approx 0.65$. While we thus can reproduce the findings of Guettari et al.[46] and Shankar et al.[47] in terms of extreme behavior at a water–alcohol mole ratio of 2:1, corresponding to maximally nonideal behavior of the solvent, we see the opposite extreme of maximum viscosity, suggesting maximum coil expansion and thus a maximally good solvent at this mixing ratio. We will return to the interpretation of this difference in the Discussion.

Given the strong variation in viscosity with water–ethanol ratio, it is clear that a c_{PAA} value suitable for electrospinning with one solvent composition may no longer be adequate if the water–ethanol ratio changes. We hypothesize that it will be possible to spin fibers with consistent quality across the full water–ethanol mixture window if we identify values of c_{PAA} for each solvent composition that yield a common viscosity η_0, which is tuned to be appropriate for electrospinning. We identify η_0 empirically by conducting preliminary electrospinning experiments using a solvent with water–ethanol ratio of 50:50 (by mass) and varying c_{PAA}. The best results (fibers with uniform diameter and few beads) are obtained with 7% w/w PAA, corresponding to $\eta \approx 700 - 800$ mPa·s at $\dot{\gamma} = 2.34\ s^{-1}$. For the other solvent compositions, we thus interpolate each relevant $\eta(\dot{\gamma})$ data set corresponding to Figures S3–S7, Supporting Information using an exponential fit to identify c_{PAA} that will yield $\eta_0 \approx 700$–800 mPa·s at $\dot{\gamma} = 2.34\ s^{-1}$. **Table 1** lists the compositions of the resulting PAA solutions prepared for electrospinning and Figure S9, Supporting Information shows the corresponding $\eta(\dot{\gamma})$ curves. The data for PAA in pure ethanol and in pure water, respectively, almost overlap at values slightly higher than η_0, while the data obtained with mixed solvents show some variations within the range 600–950 mPa s.

© 2021 The Authors. Macromolecular Materials and Engineering published by Wiley-VCH GmbH

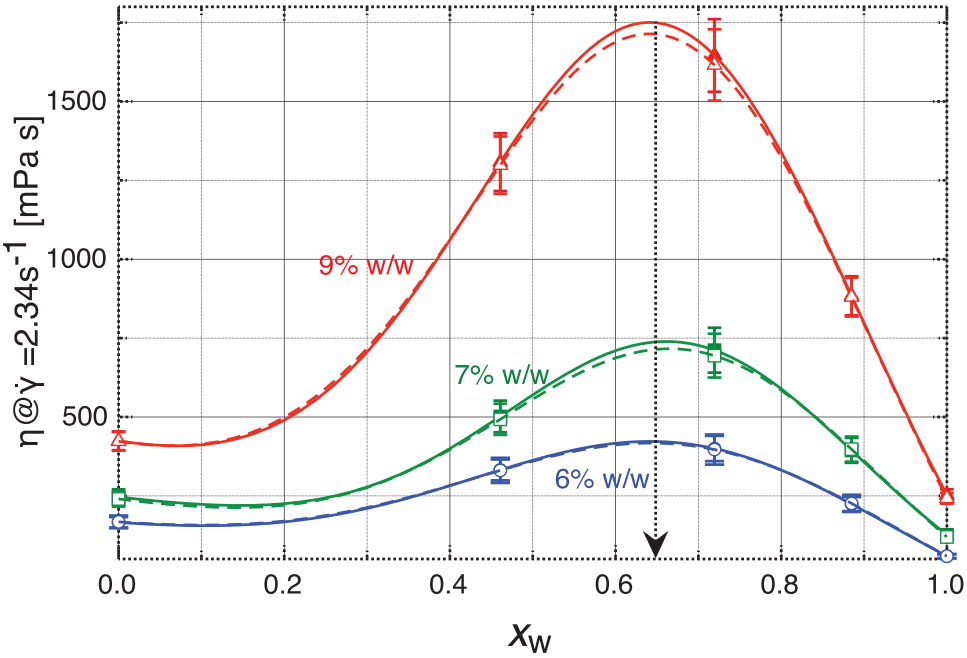

Figure 2. Low-shear rate ($\dot{\gamma}$=2.34 s^{-1}) viscosity η as a function of mole fraction of water in the ethanol–water solvent used for dissolving PAA at mass concentrations 6% , 7% , and 9% w/w, respectively. Filled symbols and continuous curves correspond to η obtained during a scan with increasing $\dot{\gamma}$, whereas empty symbols and dashed curves correspond to measurements upon decreasing $\dot{\gamma}$. The arrow highlights the solvent composition with $n_w \approx 0.65$ which appears to exhibit optimum solvent properties for PAA. The error bars are a standard deviation obtained from 4 different measurements each with increasing and decreasing shear rate.

Table 1. Concentrations (by mass) c_{PAA} of viscosity-matched solutions with different mole fractions x_w of water (or mass fractions c_w), both referring to the mixture without PAA, tailored for comparable electrospinning conditions regardless of solvent composition.

Solution	c_{PAA} [% w/w]	x_w	c_w [% w/w]
1	10	0	0
2	7.5	0.46	25
3	7	0.72	50
4	8.5	0.88	75
5	11.5	1	100

Table 2. The mean cross section diameter $\bar{d}$ with standard deviation, as obtained by measuring 100 individual cross sections in SEM images, of fibers produced from each density matched solution (compositions in Table 1), at relative humidity RH, temperature T, spinneret–collector distance L, spinning voltage V, and flow rate Q.

Solution	$\bar{d}$ [μm]	RH [%]	T [°C]	L [cm]	V [kV]	Q [mL h^{-1}]
1	2.30±0.24	29	25.1	14	7.5	0.61
2	1.30±0.13	30	24.8	14	7.5	0.65
3	1.70±0.12	30	24.5	14	7.5	0.43
4	0.67±0.06	35	26.3	14	7.5	0.23
5	1.08±0.15	35	25.9	14	7.5	0.37

2.2. Taylor Cones and Electrospun Fibers

After identifying the target viscosity η_0 and preparing PAA solutions using pure water, pure ethanol, and the three solvent mixtures, respectively, adjusting c_{PAA} to ensure $\eta \approx \eta_0$, (Table 1), we carried out electrospinning experiments to assess the suitability of each solution. The parameters for each spinning experiment are summarized in **Table 2**. During electrospinning, we paid particular attention to the Taylor cone appearance as a function of time, filming it for at least 30 s (Movies S1–S5, Supporting Information), and measuring the time that fibers are produced without the operator needing to clean the spinneret (we call this duration a "spinning cycle"). Snapshots from the beginning and end of a cycle, respectively, are shown in **Figure 3**.

Looking at the top row in Figure 3, we see that a nearideal Taylor cone develops quickly at the start of a cycle for every solution, and a stable single-jet ejection can easily be recognized in the photos. The situation is very different toward the end of a cycle, where only Solution 4 leads to a maintained stable Taylor cone and continued spinning. Although the Taylor cone in (*d′*) has grown in volume compared to (*d*), an overall stable spinning situation is seen here. For the high-ethanol content solutions 1 and 2, an unnatural distortion and elongation of the Taylor cone can be recognized, suggesting that gelation is taking place on the Taylor cone surface. Indeed, this distortion is the reason why the spinneret has to be wiped clean, ending the cycle. The distortion is present also in the Taylor cone with Solution 3, although it is not as apparent, and again this is the reason for terminating the cycle by wiping the spinneret clean.

Solution 5, where pure water is used as solvent, is different. Additionally, in this experiment, the cycle is relatively short (18 s).

© 2021 The Authors. Macromolecular Materials and Engineering published by Wiley-VCH GmbH

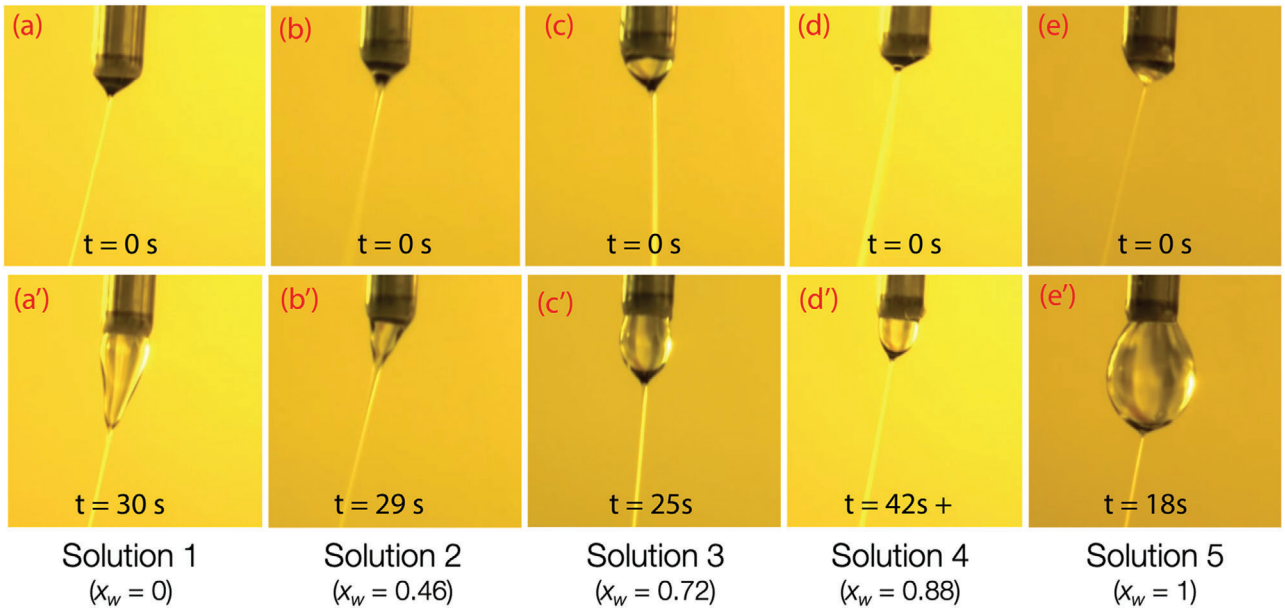

Figure 3. Taylor cone pictures of different PAA solutions (compositions in Table 1), imaged at the beginning (top row) and end (bottom row) of a spinning cycle. The spinneret was wiped clean at the end of each cycle, just after the timestamp label in the lower row, in order to restart the cycle, except for column *d*/*d*′, where spinning could continue well beyond the 42 s during which the Taylor cone was filmed (hence the t = 42 s + label in *d*′)

The reason why the spinneret has to be wiped at this point is not gelation, but rather a rapid growth of the Taylor cone to a volume where it is about to detach as a droplet. If it is not wiped off, it will land on the fiber mat and ruin the previously spun fibers. We will later return to the origin of gelation of the ethanol-rich Taylor cones and of the dramatic volume expansion of the pure-water-based Taylor cone (despite having the second lowest flow rate in the entire study, see Table 2) in the Discussion.

Our hypothesis that solutions optimized for $\eta = \eta_0$ will produce good fibers regardless of solvent composition is supported by the fact that all five solutions give smooth fibers that are free of beads, as shown in the scanning electron microscope (SEM) characterization images in **Figure 4**. However, there is a non-negligible variation of the average diameter $\bar{d}$ of the fiber cross section, spanning the range 0.6–2.3 μm. As can be seen in the histograms on the right in Figure 4 and Table 2, this variation shows a systematic correlation neither with the solvent composition x_w nor with the PAA concentration c_{PAA}. The thickest fibers are obtained with Solution 1, with a medium PAA concentration of c_{PAA} = 10% w/w at one end of the solvent composition scale, at $x_w = 0$, but the thinnest fibers are not obtained at the opposite end, but at $x_w = 0.88$. The fibers at $x_w = 1$, corresponding to the maximum PAA content c_{PAA} = 11.5% w/w, are among the thinner in the study, contrasting significantly to those obtained with $x_w = 0$ although these two solutions showed almost identical η in Figure S9, Supporting Information. The flow rate Q has significant impact, the thinnest fibers being spun with the lowest flow rate (Table 2), but there are inconsistencies also here. For instance, the greatest flow rate (Q = 0.65 mL h^{-1}) was used for Solution 2, but this produced significantly less thick fibers than Solution 1 pumped at Q = 0.61 mL h^{-1}. We will attempt to resolve these surprising and apparent inconsistencies in the following section.

3. Discussion

We first address the maximum in PAA solution viscosity at intermediate water–ethanol mixing ratios, and the maximally expanded coil size that can be assumed from this behavior. The mixing of ethanol and water is a classic example of non-ideal mixing behavior,[51–53] with a maximally negative excess volume at a water mole fraction that is often located at $x_w \approx 0.6$,[53,54] although Belda et al. report a higher value of $x_w = 0.75$.[55] This behavior is attributed to the clathrate caging of ethanol molecules by surrounding water molecules in order to maximize the number of hydrogen bonds of the latter, maximizing the enthalpy of mixing at the cost of reduced entropy, as the caging reduces the configuration space for hydrogen bonding of the water molecules.[56] The maximum deviation from ideal mixing behavior can also be seen in a maximum of viscosity of ethanol–water mixtures at $x_w \approx 0.7$.[57] However, this viscosity maximum is three orders of magnitude lower than that of the PAA solutions studied here; the impact of the viscosity of the solvent itself is thus negligible in the context of our study.

We note that the most common value $x_w \approx 0.6$[54] for maximum non-ideal water–ethanol mixing coincides rather well with $x_w \approx 0.65$ for maximum PAA solution viscosity seen in Figure 2, as well as with the minimum of solvent quality for PVP in ethanol–water mixtures studied by Guettari et al.[46] Based on dielectric spectroscopy data, Sato et al. concluded that a first critical mole fraction is $x_w = 0.82$, at which the excess activation free energy €G^E is at a maximum, corresponding to maximum ethanol–water interactions.[52] They argue that, for lower x_w, ethanol molecules form clusters, thus with microphase segregation taking place between water and ethanol. They found a second critical mole fraction of $x_w = 0.58$, near the region where most studies find the maximum negative excess volume,[54] which they

© 2021 The Authors. Macromolecular Materials and Engineering published by Wiley-VCH GmbH

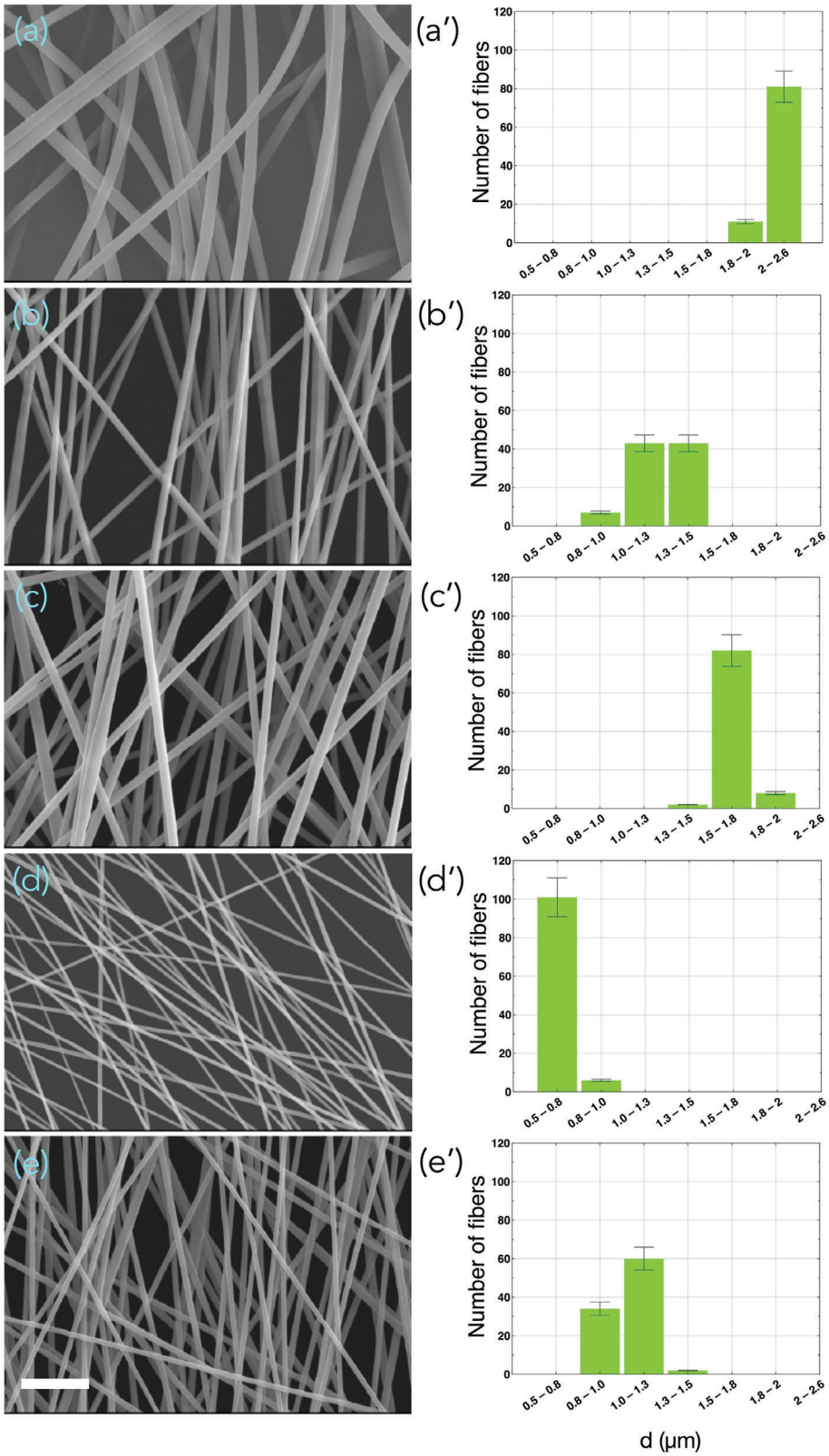

Figure 4. Left column: representative SEM images of the fibers produced from each of the five viscosity-matched solutions (compositions in Table 1). Scale bar 5 μm. Right column: histograms showing the distribution of cross section diameters d of fibers spun from each solution. The corresponding Taylor cone movies are provided in Supporting Information, and key snapshots are shown in Figure 3.The error bars on the histograms represent standard deviation.

© 2021 The Authors. Macromolecular Materials and Engineering published by Wiley-VCH GmbH

attribute to this microphase segregation reaching its maximum, linking it to Ben-Naim's identification of this mole fraction as having maximum affinity of ethanol molecules but minimum affinity between ethanol and water.[51] We can thus conclude that the mole fraction where we find a maximum PAA solution viscosity corresponds to the conditions where the ethanol–water mixture is the furthest from ideal, with a microphase segregation of water and ethanol which is at its maximum.

The key remaining question is why this extreme condition yields maximum viscosity of PAA solutions, suggesting maximally expanded coils and an optimum solution behavior for PAA, whereas the same solvent mixture shows an extreme in poor solvent behavior for PVP.[46] We assume that this is related to the ionizable acid groups of PAA and the fact that the counter ions of the carboxyl pendants of PAA are protons (H^+), rendering the degree of ionization highly sensitive to pH. The acidic nature of PAA thus itself influences its degree of deprotonation. For aqueous PAA solutions set to pH <5 by a low molar mass acid, Swift et al. found the deprotonation of the carboxyl groups to be negligible.[58] In our case, pH<5 for $c_{PAA} \geq 6\%$ w/w for all x_w (see Figure S10, Supporting Information), which means that the average degree of ionization of PAA must be low, explaining why ethanol is overall the better solvent. Indeed, we find a slight turbidity in the solutions with high water content, whereas those with high ethanol content are clear (Figure S11, Supporting Information). However, the low pH comes from protonation of PAA in the first place; hence, ionization up to a saturation fraction does occur along the chains. This gives them polyelectrolyte character with electrostatic self repulsion along the polymer chain, increasing the persistence length and therefore expanding the coil in solution. As the ethanol fraction of the solvent increases, pH also increases, reflecting the expected reduced degree of ionization as the solvent permittivity decreases. This means a decreasing electrolyte character, with a consequent reduced impact of electrostatic coil expansion. The variation of PAA ionization should be reflected by a corresponding variation of solution conductivity, which would suggest that the fiber thickness increases with ethanol content, as high conductivity is known to decrease the fiber diameter.[1–5] However, the results in Figure 4 show a dependence on solvent composition that is not fully systematic, suggesting that the conductivity impact is overlaid by other effects, to be discussed below.

We conjecture that the maximum viscosity at constant c_{PAA} at $n_w \approx 0.65$ is a result of maximally expanded coils because of all the different aspects influencing the PAA chain interactions contributing synergistically at this apparently optimum solvent mixture composition. The benefit of water's ability to deprotonate the PAA is combined with ethanol's ability to solubilize the protonated residues (in majority), and the partial charging of the polymer expands the coil via the electrostatically increased persistence length. These effects are then amplified by the fact that the entropic penalty of microphase segregation of ethanol and water is maximized at $w_x \approx 0.6$.[52] The presence of partially ionized PAA could reduce the free energy of the solvent by having the water molecules interacting mainly with deprotonated acid groups while the ethanol interacts mainly with the protonated ones and the polymer backbone, as has indeed been suggested by molecular dynamics simulations.[59] In other words, the polymer–solvent interactions are particularly strong at $w_x \approx 0.6$, as each fraction of the polymer, protonated and deprotonated, respectively, interacts preferentially with one of the two solvent species, reducing the entropy penalty of direct ethanol–water interaction at this maximally nonideal mixing ratio. Hammouda et al. also found that a mixture of ethanol and water promotes PAA dissolution[60] and they also attributed the effect to a molecular scale solvent segregation. However, their conjecture that water dissolves mainly the carboxylate groups—regardless of degree of deprotonation—whereas the ethanol dissolves mainly the backbone would suggest that water–alcohol mixtures would be better solvents also for PVP and PEO, in contradiction with the findings of Guettari et al.[46] and Shankar et al.[47] Future more detailed investigations, in particular involving computer simulations, are needed to gain a full understanding of the phenomena.

Next, we attempt to explain the apparently unsystematic variations in fiber cross section diameter $\bar{d}$ between the five solutions used for electrospinning seen in Figure 4 and Table 2. We believe that this is due to the fact that the impact on the electrospinning results of η—which is similar for all five solutions as they were prepared—is dwarfed by the changes to the solvent composition taking place over time in the Taylor cone. This thus gives rise to the significant variations in cycle length and Taylor cone shape seen in Figure 3, but it also impacts the characteristics of the fibers that finally end up on the collector. We recently found that the cooling due to ethanol evaporation from the Taylor cone of an ethanolic PVP solution electrospun in a humid atmosphere leads to significant water condensation, which—counterintuitively—leads to gelation of the Taylor cone surface and disruption of the electrospinning process.[40] This surprising finding can be understood from the fact that water condensation actually accelerates ethanol or methanol evaporation due to the latent heat released when water condenses.[61]

We believe the same phenomenon is at play here, despite a significantly lower atmospheric humidity. Most likely, the well-known hygroscopic nature of PAA (the most common application of PAA is as a superabsorbant material due to its ability to absorb water and swell to many times its own volume) contributes to an extreme sensitivity to humidity, the PAA effectively promoting water condensation and thus triggering the enhanced ethanol evaporation. This explains why the outer surface of the Taylor cone of PAA in pure ethanol gels so quickly, terminating the spinning cycle after about 30 s in Figure 3, and it also explains why the Taylor cone always grows in volume over time within a spinning cycle, despite the flow rate being slightly lower than typical for electrospinning. In fact, Q was as low as possible in all experiments, any further reduction effectively stopping the initial Taylor cone development. If water is present in the spinning solution from the start, the impact on ethanol evaporation is reduced in magnitude, but the gelation of the Taylor cone is nevertheless strong enough to also terminate the cycle in spinning experiments with Solutions 2 and 3.

With Solution 5, there is no ethanol that can evaporate, as the solvent is pure water. In this case, consequently, the cycle is not terminated by surface gelation of the Taylor cone, but by an extreme growth of the droplet protruding from the spinneret to the point that it can hardly be described as a Taylor cone any more and where an operator must remove it in order to avoid dripping onto the fiber mat. It must be emphasized that this is not due to overfeeding because of too high flow rate; Q is the second lowest in

© 2021 The Authors. Macromolecular Materials and Engineering published by Wiley-VCH GmbH

the study for Solution 5. Rather, we believe it is the fact that c_{PAA} is the highest of all solutions, in order to reach the targeted η_0 in this nonoptimum solvent. The large PAA loading leads to maximum impact of the hygroscopic nature of PAA, drawing in additional water from the air as spinning proceeds. While it may seem surprising that PAA could act to draw in additional water from the air when it already is in solution, one should be aware that significant phase separation takes place during electrospinning in the Taylor cone, near the apex from which the jet is ejected.[62] This means that the PAA concentration can be high locally, allowing it to absorb additional water at these locations.

We believe the low value of $\bar{d}$ seen when spinning solution 4 is the one truly representative of the viscosity-matched solutions. This solution has a quite low c_{PAA}, reducing the impact of its hygroscopic nature, and a relatively low ethanol content, eliminating the risk of Taylor cone gelation due to water condensation. The other fibers have $\bar{d}$ that are more determined by the dynamic variations of the PAA solution at the Taylor cone surface during spinning, due to water condensing from the air.

4. Conclusion

While PAA dissolves in ethanol as well as water, or any mixture of the two, its behavior changes in a highly nonlinear and nontrivial way as the solvent composition is varied. Surprisingly, the viscosity η at constant PAA concentration c_{PAA} is maximum at a water-to-ethanol mole fraction of $x_w \approx 0.65$, corresponding to maximum deviation from ideal mixing behavior of water and ethanol. We believe it provides a synergistic combination of partial deprotationation of carboxylate groups by water while the ethanol dissolves the remaining uncharged polymer fraction. Having established how η varies with x_w we find that consistent electrospinning of PAA solutions of any water–ethanol solvent ratio can be initiated with $\eta \approx 0.7$ Pa s, but the fiber cross section diameter varies in apparently inconsistent ways, and the spinneret must be regularly wiped clean, due to an unavoidable rapid growth of the Taylor cone and/or gelation in case of ethanol-rich solutions. We attribute this behavior to the extreme hygroscopic nature of PAA, leading to significant water condensation into the Taylor cone despite a spinning atmosphere with moderate relative humidity. This demonstrates the vital importance of monitoring the Taylor cone quality over time during electrospinning and paying attention to any unexpected processes taking place there, which may impact the electrospinning process.

5. Experimental Section

Polymer Solutions: Poly(acrylic acid) (PAA; $M_w = 450$ kg mol^{-1}) was purchased from Sigma-Aldrich and dissolved in anhydrous ethanol (99%, from VWR) for solutions in pure ethanol, ultrapure deionized water (conductivity 0.055 μS cm^{-1} Sartorius Arium) for solutions in pure water, or mixtures of the two solvents. Multiple PAA solutions were prepared, with various selected concentrations c_{PAA} (by mass), in water–ethanol mixtures of 0, 25, 50, 75, and 100% w/w ratio. All materials were used as received without further purification.

Viscosity Measurements: The oscillatory shear viscosity η was measured in plate-plate geometry (50 mm diameter, 1.0 mm gap) using an Anton Paar rheometer (MRC-102), controlled by Rheocompass software. The shear rate $\dot{\gamma}$ was swept from 0.1 to 10 s^{-1} and then back to 0.1 s^{-1}. All the measurements were performed at room temperature (25 °C), using a solvent trap to prevent ethanol from evaporating during the measurements.

Electrospinning: The electrospinning setup (vertical geometry, schematic in Figure S1, Supporting Information) was housed inside a closed acrylic box in order to ensure a well-defined spinning atmosphere. An 18-gauge blunt-tipped disposable stainless steel needle (outer diameter 1.20 mm), purchased from VWR, was used as the spinneret, mounted in the top of the acrylic box. To apply the electric field to drive spinning, the spinneret was connected to a high voltage power supply (Gamma High Voltage, model ES30R-5W/DAM/RS232) while the collector was grounded. The PAA solution to be spun was pumped to the spinneret using a microfluidic pressure controller (Fluigent, model MFCS-EZ, maximum pressure 1034 mbar, uncertainty ± 0.3 mbar). The Taylor cone was imaged using a digital camera (Pixelink D755) equipped with a macro lens (Tokina AT-X Pro).

For all experiments, a spinneret–collector distance of 14 cm and a spinning voltage of 7.5 kV were chosen. The temperature T and relative humidity RH were monitored during all experiments, and the flow rate Q was adjusted for maximally stable spinning for each solution. Fibers were collected freely hanging on an untreated copper wire frame.

Electron Microscopy Characterization: The fibers were characterized using a JEOL JSM-6010LA SEM (Akishima, Japan), operated at 20 kV with a working distance of 11 mm. Prior to imaging, the fibers were coated with gold (≈5 nm thickness) using a sputter coater (Quorum Q150R ES) for 100 s. The fiber cross section diameter was established by randomly selecting at least 100 fibers from the SEM images and measuring the apparent cross section using the software ImageJ (NIH, USA).

Supporting Information

Supporting Information is available from the Wiley Online Library or from the author.

Acknowledgements

Funding for this research was provided by a European Research Council Consolidator Grant (INTERACT, grant number 648763) and by an *Aide à la formation-recherche* grant (LIMEFLOW, grant number 9784104) from the Luxembourg National Research Fund. The authors thank Nicolas Tournier, Dr. Ulrich M. Siegel, Dr. Catherine G. Reyes, and Dr. Hakam Agha for assistance in constructing the experimental set-up; Dr. Alex Gansen, Claudius M. Lehr, Dr. Jörg Baller, and Prof. Jeanne H. Norton for assistance with the rheological characterization; Zornitza Tosheva for helping with SEM imaging and pH measurements; and Dr. Manos Anyfantakis and Dr. V.S.R. Jampani for fruitful discussions.

Conflict of Interest

The authors declare no conflict of interest.

Data Availability Statement

The data that support the findings of this study are available from the corresponding author upon reasonable request.

Keywords

electrospinning, ethanol, poly(acrylic acid), polymers, solvents, viscosity, water

Received: August 27, 2021
Revised: October 29, 2021
Published online:

© 2021 The Authors. Macromolecular Materials and Engineering published by Wiley-VCH GmbH

[1] S. Ramakrishna, K. Fujihara, W.-E. Teo, T.-C. Lim, Z. Ma, *An Introduction to Electrospinning and Nanofibers Electrospinning Process*, Vol. *3*, World Scientific, Singapore **2005**.
[2] G. Rutledge, S. Fridrikh, *Adv. Drug Delivery Rev.* **2007**, *59*, 1384.
[3] D. Reneker, A. Yarin, *Polymer* **2008**, *49*, 2387.
[4] J. H. Wendorff, S. Agarwal, A. Greiner, *Electrospinning: Materials, Processing, and Applications*, Wiley-VCH, Weinheim **2012**.
[5] J. Xue, T. Wu, Y. Dai, Y. Xia, *Chem. Rev.* **2019**.
[6] M. Urbanski, C. G. Reyes, J. Noh, A. Sharma, Y. Geng, V. S. R. Jampani, J. P. F. Lagerwall, *J. Phys.: Condens. Matter* **2017**, *29*, 133003.
[7] J. H. Park, G. C. Rutledge, *Macromolecules* **2017**, *50*, 5627.
[8] M. Jasiurkowska-Delaporte, E. Juszyńska-Gałązka, W. Sas, P. M. Zieliński, A. Baranowska-Korczyc, *J. Mol. Liq.* **2021**, *331*, 115817.
[9] A. E. Mamuk, Ç. Koçak, Ç. E. Demirci Dönmez, *Colloid Polym. Sci.* **2021**.
[10] K. T. Dicker, D. Ratchford, R. Casalini, M. D. Thum, J. H. Wynne, J. G. Lundin, *Langmuir* **2020**, *36*, 7916.
[11] G. Scalia, E. Enz, O. Calò, D. K. Kim, M. Hwang, J. H. Lee, J. P. F. Lagerwall, *Macromol. Mater. Eng.* **2013**, *298*, 583.
[12] D. K. Kim, M. Hwang, J. P. F. Lagerwall, *J. Polym. Sci., Part B: Polym. Phys.* **2013**, *51*, 855.
[13] E. Enz, V. La Ferrara, G. Scalia, *ACS Nano* **2013**, *7*, 6627.
[14] A. L. Medina-Castillo, J. F. Fernández-Sánchez, A. Fernández-Gutiérez, *Adv. Funct. Mater.* **2011**, *21*, 3488.
[15] E. Enz, J. P. F. Lagerwall, *J. Mater. Chem.* **2010**, *20*, 6866.
[16] E. Enz, U. Baumeister, J. Lagerwall, *Beilstein J. Org. Chem.* **2009**, *5*, 58.
[17] J. P. F. Lagerwall, J. T. McCann, E. Formo, G. Scalia, Y. Xia, *Chem. Commun.* **2008**, *42*, 5420.
[18] J. E. Díaz, A. Barrero, M. Márquez, I. G. Loscertales, *Adv. Funct. Mater.* **2006**, *16*, 2110.
[19] P. Rathore, J. Schiffman, *ACS Appl. Mater. Interfaces* **2021**, *13*, 48.
[20] D. Han, A. Steckl, *Chempluschem* **2019**, *84*, 1453.
[21] A. Yarin, *Polym. Adv. Technol.* **2011**, *22*, 310.
[22] L. Bellan, H. Craighead, *Polym. Adv. Technol.* **2011**, *22*, 304.
[23] J. Wang, A. Jákli, J. L. West, *J. Mol. Liq.* **2018**, *267*, 490.
[24] J. Wang, A. Jákli, J. West, *ChemPhysChem* **2016**, *17*, 3080.
[25] E. A. Buyuktanir, M. W. Frey, J. L. West, *Polymer* **2010**, *51*, 4823.
[26] S. Ji, Y. Li, M. Yang, *Sens. Actuators, B* **2008**, *133*, 644.
[27] Y. Kye, C. Kim, J. P. F. Lagerwall, *J. Mater. Chem. C* **2015**, *3*, 8979.
[28] C. G. Reyes, A. Sharma, J. P. F. Lagerwall, *Liq. Cryst.* **2016**, *43*, 1986.
[29] L. Pschyklenk, T. Wagner, A. Lorenz, P. Kaul, *ACS Appl. Polym. Mater.* **2020**, *2*, 1925.
[30] M. J. Bertocchi, P. Vang, R. B. Balow, J. H. Wynne, J. G. Lundin, *ACS Appl. Polym. Mater.* **2019**, *1*, 2068.
[31] M. D. Thum, D. C. Ratchford, R. Casalini, J. H. Wynne, J. G. Lundin, *ACS Appl. Nano Mater.* **2021**, *4*, 297.
[32] N. Wang, H. Chen, L. Lin, Y. Zhao, X. Cao, Y. Song, L. Jiang, *Macromol. Rapid Commun.* **2010**, *31*, 1622.
[33] J. McCann, M. Marquez, Y. Xia, *Nano. Lett.* **2006**, *6*, 2868.
[34] J. Park, P. Braun, *Adv. Mater.* **2009**, *22*, 496.
[35] B. Pant, M. Park, S.-J. Park, *Pharmaceutics* **2019**, *11*, 305.
[36] K. Khoshnevisan, H. Maleki, H. Samadian, S. Shahsavari, M. Sarrafzadeh, B. Larijani, F. Dorkoosh, V. Haghpanah, M. Khorramizadeh, *Carbohydr. Polym.* **2018**, *198*, 131.
[37] S. Chou, D. Carson, K. Woodrow, *J. Controlled Release* **2015**, *220*, 584.
[38] W. Ji, Y. Sun, F. Yang, J. van den Beucken, M. Fan, Z. Chen, J. Jansen, *Pharm. Res.* **2011**, *28*, 1259.
[39] A. Saraf, L. Baggett, R. Raphael, F. Kasper, A. Mikos, *J. Controlled Release* **2010**, *143*, 95.
[40] C. G. Reyes, J. P. Lagerwall, *ACS Appl. Mater. Interfaces* **2020**, *12*, 26566.
[41] K. Terao, in *Encyclopedia of Polymeric Nanomaterials* (Eds: S. Kobayashi, K. Müllen), Springer, Berlin, Heidelberg **2021**, pp. 1–6.
[42] J. O. Iroh, in *Polymer Data Handbook* (Ed: J. Mark), Oxford University Press, New York **1999**, pp. 558–560.
[43] L. Li, Y. Hsieh, *Nanotechnology* **2005**, *16*, 2852.
[44] Y. B. Truong, J. Choi, J. Mardel, Y. Gao, S. Maisch, M. Musameh, I. L. Kyratzis, *Macromol. Mater. Eng.* **2017**, *302*, 1700024.
[45] I. Ismail, N. Bakar, T. Ling, N. Ideris, Z. Zain, N. Radacsi, *Mater. Today: Proc.* **2019**, *17*, 574.
[46] M. Guettari, A. Belaidi, S. Abel, T. Tajouri, *J. Solution Chem.* **2017**, *46*, 1404.
[47] R. Shankar, R. R. Klossner, J. T. Weaver, T. Koga, J. H. van Zanten, W. E. Krause, C. M. Colina, F. Tanaka, R. J. Spontak, *Soft Matter* **2009**, *5*, 304.
[48] G. Smolyakov, J.-M. Catala, N. Kutsevol, M. Rawiso, in *Modern Problems of Molecular Physics* (Eds: L. A. Bulavin, A. V. Chalyi), Springer, Cham **2018**, pp. 133–147.
[49] X. Meng, Y. Du, Y. Liu, E. B. Coughlin, S. L. Perry, J. D. Schiffman, *Macromolecules* **2021**, *54*, 5033.
[50] S. K. Tiwari, S. S. Venkatraman, *Mater. Sci. Eng.: C* **2012**, *32*, 1037.
[51] A. Ben-Naim, *J. Chem. Phys.* **1977**, *67*, 4884.
[52] T. Sato, A. Chiba, R. Nozaki, *J. Chem. Phys.* **1999**, *110*, 2508.
[53] J. Ott, J. Sipowska, M. Gruszkiewicz, A. Woolley, *J. Chem. Thermodyn.* **1993**, *25*, 307.
[54] I. Abdulagatov, L. A. Akhmedova-Azizova, N. Azizov, *Fluid Phase Equilib.* **2014**, *376*, 1.
[55] R. Belda, J. V. Herráez, O. Diez, *Phys. Chem. Liq.* **2004**, *42*, 467.
[56] D. Chandler, *Nature* **2005**, *437*, 640.
[57] S. Song, C. Peng, *J. Dispersion Sci. Technol.* **2008**, *29*, 1367.
[58] T. Swift, L. Swanson, M. Geoghegan, S. Rimmer, *Soft Matter* **2016**, *12*, 2542.
[59] S. Srikant, S. S. Muralidharan, U. Natarajan, *Mol. Simul.* **2013**, *39*, 145.
[60] B. Hammouda, F. Horkay, M. L. Becker, *Macromolecules* **2005**, *38*, 2019.
[61] C. Law, T. Xiong, C. Wang, *Int. J. Heat Mass Transfer* **1987**, *30*, 1435.
[62] C. Wang, T. Hashimoto, *Macromolecules* **2020**, *53*, 9584.

 © 2021 The Authors. Macromolecular Materials and Engineering published by Wiley-VCH GmbH